Multibody system modelling of unmanned aircraft system collisions with the human head

Rattanagraikanakorn, Borrdephong; Gransden, Derek I.; Schuurman, Michiel; de Wagter, Christophe; Happee, Riender; Sharpanskykh, Alexei; Blom, Henk

DOI
10.1080/13588265.2019.1633818

Publication date
2019

Document Version
Final published version

Published in
International Journal of Crashworthiness

Citation (APA)
Rattanagraikanakorn, B., Gransden, D. I., Schuurman, M., de Wagter, C., Happee, R., Sharpanskykh, A., & Blom, H. (2019). Multibody system modelling of unmanned aircraft system collisions with the human head. *International Journal of Crashworthiness*, *25 (2020)*(6), 689-707. https://doi.org/10.1080/13588265.2019.1633818

International Journal of Crashworthiness

ISSN: 1358-8265 (Print) 1754-2111 (Online) Journal homepage: https://www.tandfonline.com/loi/tcrs20

Multibody system modelling of unmanned aircraft system collisions with the human head

Borrdephong Rattanagraikanakorn, Derek I. Gransden, Michiel Schuurman, Christophe De Wagter, Riender Happee, Alexei Sharpanskykh & Henk A. P. Blom

To cite this article: Borrdephong Rattanagraikanakorn, Derek I. Gransden, Michiel Schuurman, Christophe De Wagter, Riender Happee, Alexei Sharpanskykh & Henk A. P. Blom (2019): Multibody system modelling of unmanned aircraft system collisions with the human head, International Journal of Crashworthiness, DOI: 10.1080/13588265.2019.1633818

To link to this article: https://doi.org/10.1080/13588265.2019.1633818

Published online: 27 Jul 2019.

INTERNATIONAL JOURNAL OF CRASHWORTHINESS
https://doi.org/10.1080/13588265.2019.1633818

Taylor & Francis
Taylor & Francis Group

Multibody system modelling of unmanned aircraft system collisions with the human head

Borrdephong Rattanagraikanakorn[a], Derek I. Gransden[b], Michiel Schuurman[a], Christophe De Wagter[c], Riender Happee[d], Alexei Sharpanskykh[e] and Henk A. P. Blom[e]

[a]Aerospace Structures & Materials Department, Faculty of Aerospace Engineering, Delft University of Technology, Delft, The Netherlands; [b]Bharti School of Engineering, Laurentian University, Sudbury, Canada; [c]MavLab, Faculty of Aerospace Engineering, Delft University of Technology, Delft, The Netherlands; [d]Cognitive Robotics, Mechanical Engineering, Delft University of Technology, Delft, The Netherlands; [e]Section Air Transport and Operation, Faculty of Aerospace Engineering, Delft University of Technology, Delft, The Netherlands

ABSTRACT

Understanding the impact severity of unmanned aircraft system (UAS) collisions with the human body remains a challenge and is essential to the development of safe UAS operations. Complementary to performing experiments of UAS collisions with a crash dummy, a computational impact model is needed in order to capture the large variety of UAS types and impact scenarios. This article presents the development of a multibody system (MBS) model of a collision of one specific UAS type with the human body as well with a crash dummy. This specific UAS type has been chosen because data from experimental drop tests on a crash dummy is available. This allows the validation of the MBS model of UAS impacting a crash dummy versus experimental data. The validation shows that the MBS model closely matches experimental UAS drop tests on a crash dummy. Subsequently, the validated UAS MBS model is applied to predict human body injury using a biomechanical human body model. Head and neck injury from the frontal, side and rear impact on the human head are predicted at various elevation angles and impact velocities. The results show that neck injury is not a concern for this specific UAS type, but a serious head injury is probable.

ARTICLE HISTORY
Received 22 February 2019
Accepted 13 June 2019

KEYWORDS
UAS; drone; impact; human; injury

1. Introduction

UAS (or unmanned aircraft system) operations have received much attention in the past few years and will soon become a critical part in aviation. Low-level UAS operations will likely be operated in an urban environment where population density is high. While this type of operations may pose a serious collision risk to people on the ground, the level of severity of UAS collisions on a human is not yet fully understood. This lack of understanding affects rules and regulations, as well as any necessary mitigative measures, to be established in order to prevent fatal accidents. EASA [1] has published prototype rules and regulations for UAS operations; nevertheless, additional scientific results are still required to support UAS requirements. As stated by EASA [2], there is still an urgent need to investigate UAS collision risks using experimentation and validated analytical models.

Several research groups have investigated the effect of UAS collisions on different actors on the ground. Civil Aviation Safety Authority and Monash University [3] proposed a simplified injury prediction model for the impact of small UAS on a person on the ground to determine a non-lethal UAS mass. The model predicted the severity level from blunt force trauma injuries based on the impacting projectile's kinetic energy and impact diameter. Another modelling approach was proposed by Magister [4] to assess small UAS injury biomechanics resulting from blunt ballistic impact. Nevertheless, such simplified energy-based models were not sufficient to provide physical insights into how UAS collision may inflict injury. To better understand UAS collision consequences, ASSURE conducted a series of impact drop test using DJI Phantom III on FAA Hybrid III crash dummy at various impact attitude and speed [5–7]. Koh et al. [8,9] also conducted extensive drop tests and computational crash simulations of different drone weight classes on a crash dummy head. In addition, Campolettano et al. [10] performed a series of live flight test and impact drop test using three different UAS weight classes on an instrumented Hybrid III crash dummy. The aim of the test was to estimate the range of injury risks to humans due to UAS impact.

The relatively high costs of live impact testing make it difficult to cover various impact conditions (e.g. impact direction, attitude or speed) and to conduct sensitivity analysis. Such difficulties can be overcome by using a computational model. For modelling and analysis of crashworthiness of aircraft parts, the finite element modelling (FEM) approach is typically adopted. However, for modelling and assessment of human injury in automotive and aerospace crashworthiness,

CONTACT Borrdephong Rattanagraikanakorn b.rattanagraikanakorn@tudelft.nl

not FEM but multibody system (MBS) modelling is widely used [11–14]. An MBS model consists of masses, springs and dampers. SOMLA [15] and MADYMO [16] are examples of a MBS-based computer codes widely used for occupant impact simulation. In spite of the physiological simplifications of MBS relative to FEM, research has shown that for human injury modelling MBS can offer similar results compared to FEM. FEM is most effective when the modelling problem requires a high-fidelity model that can capture non-linear material (tissue) local deformation and damage. However, UAS to human collision does not require such level of detail in order to approximate injury level sustained from a collision. Typically, overall kinematics of the human body (e.g. head acceleration) is needed to approximate, for example, head or neck injury level through various injury criterions.

Therefore, the aim of this article is to develop an MBS model of a typical UAS that can be used for crash simulation against a crash dummy or the human body. This article is organised as follows. Section 2 describes the modelling process of the UAS MBS model, and a description of the human body and crash dummy models used in the simulation. Section 3 presents the validation of the MBS model. Section 4 describes a crash simulation of the MBS model on the human body and the injury severity of the human body. Section 5 and 6 present the discussion of the results and the conclusion, respectively.

2. MBS models

2.1. UAS MBS modelling

The specific UAS considered is the DJI Phantom III, shown in Figure 1(a). For this UAS, a MBS model was developed, which is shown in Figure 1(b). In order to develop the model, impact footage from ASSURE [17] was investigated to identify a necessary number of body and joint, as well as joint type. The model is developed based on an assumption that there is no breakage of DJI Phantom III parts. The MBS model of the DJI Phantom III comprises of seven rigid bodies that are connected by restraint joints and dampers. The main body which includes the mainframe, avionic system and battery were lumped into Body 3. Four motors at the end of each arm were lumped into 4 bodies, which are Body 4, 5, 6 and 7. Body 2 was a lumped mass of the damp plate and avionic system for gimbal/camera control. Lastly, Body 1 was a lumped mass of the camera body and the gimbal.

The ellipsoid surface was used to model external surfaces of the DJI Phantom III drone and for contact detection and calculation. Ellipsoid surface uses force-penetration contact model to account for an interaction between the surfaces which allows the UAS model to interact with a crash dummy or the human body models in MADYMO. Kinematic joints connect bodies together while fixing the specific degrees of freedom for each body. Figure 2 illustrates rigid masses and dimensions of each segment as well as joint positions. As summarized in Table 1, three types of joints were used in this model, namely translational-revolute for Joint 1, translational for Joint 2 and universal for Joints 3–6. At each joint, Kelvin restraints (translational spring parallel with a damper) or Cardan restraints (torsional spring parallel with a damper) were implemented to account for force deflections from structural deformations.

Notice that the landing gear is not included in this DJI Phantom III MBS model. The footage analysis shows large lateral deflection of the landing gears (or skids) upon impact with the dummy head. In the collinear impact case considered, the gap between two landing gears is larger than the width of the head, resulting in no direct contact of the landing gears to the head. Also, based on preliminary stiffness tests on different components, the landing gears are made of thin ABS plastic structure which is softer than other components on the DJI Phantom III UAS. An analysis of a simplified lumped-parameter mass (LPM) model shows that the impact force on the head due to landing gear as a point of contact is non-prominent and smaller than frontal body or gimbal contacts. Therefore, the landing gears are excluded from this specific DJI Phantom III UAS model.

2.2. UAS vehicle parameters

Important UAS vehicle parameters, which are mass, the moment of inertia and geometrical dimensions of the UAS

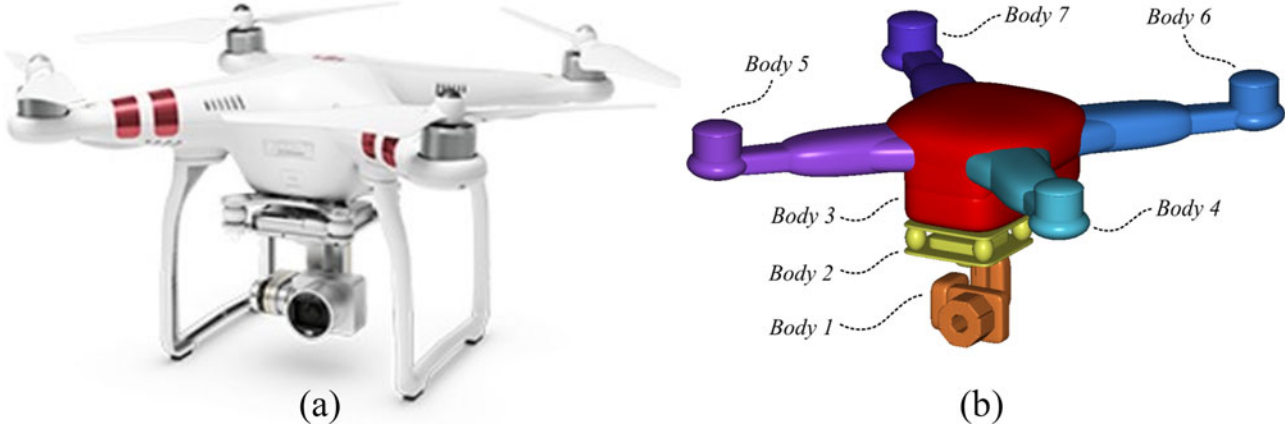

Figure 1. DJI Phantom III UAS considered for impact modelling: (a) real-world system and (b) MBS model. Notice that the two landing skids are not modelled because these are not in contact with the human head under the impact cases that are investigated.

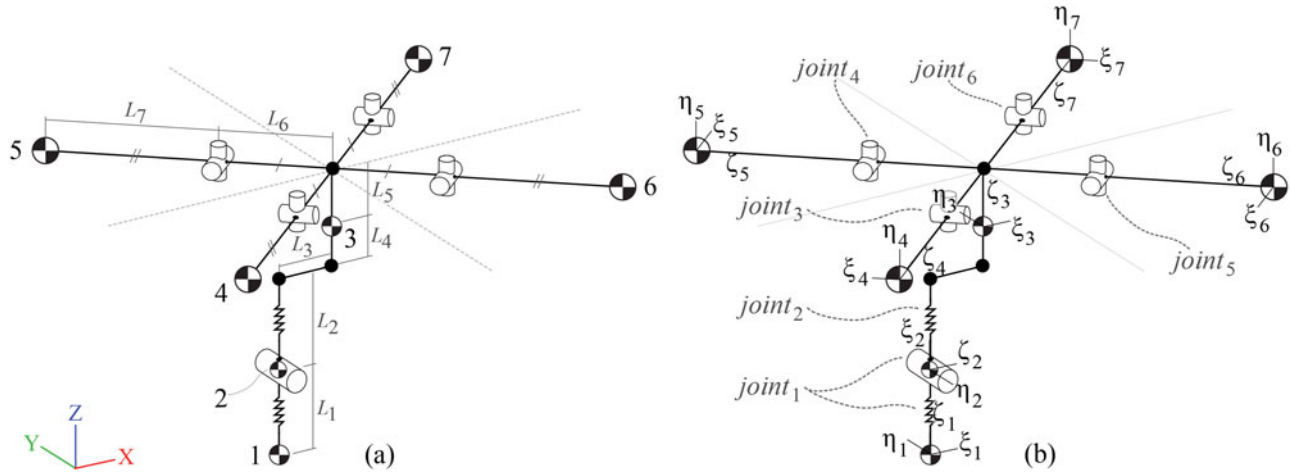

Figure 2. Skeletons of the MBS model of a DJI Phantom III UAS showing rigid masses, joints and restraints. (a) Illustrates rigid masses, and dimensions of each segment and (b) shows joint positions and local referential locations.

Table 1. Kinematic joint descriptions for UAS multibody system model.

Joint	Type	Description
1	Translational-revolute	Damp plate – Camera gimbal
2	Translational	Mainframe – Damp plate
3–6	Universal	Mainframe – Motor arm

Table 2. Summary of UAS vehicle parameters which were obtained experimentally.

Body	Mass (kg)	Moment of inertia (kg m^2)
1	0.101	$I_{XX} = 1.8 \times 10^{-7}$, $I_{YY} = 1.2 \times 10^{-7}$, $I_{ZZ} = 1.8 \times 10^{-7}$
2	0.056	$I_{XX} = 2.3 \times 10^{-6}$, $I_{YY} = 2.3 \times 10^{-6}$, $I_{ZZ} = 1.9 \times 10^{-10}$
3	0.839	$I_{XX} = 4.9 \times 10^{-3}$, $I_{YY} = 5.3 \times 10^{-3}$, $I_{ZZ} = 9.4 \times 10^{-3}$
4, 5, 6, 7	0.055	$I_{XX} = 4.4 \times 10^{-7}$, $I_{YY} = 4.4 \times 10^{-7}$, $I_{ZZ} = 6.0 \times 10^{-8}$

Table 3. Summary geometrical dimensions of the UAS.

Segment	Length (m)	Segment	Length (m)
l_1	0.044	l_5	0.030
l_2	0.020	l_6	0.014
l_3	0.023	l_7	0.165
l_4	0.016		

were obtained experimentally using the real UAS. Masses of rigid bodies were measured directly on a weight scale and bifilar tests were performed to estimate the moment of inertia of each body. Geometrical dimensions were obtained directly from physical measurements of a DJI Phantom III. Table 2 shows the summary of UAS masses and moment of inertias and Table 3 shows the summary of geometrical dimensions of the UAS.

2.3. Calibration of UAS MBS model

To model a UAS during an impact event, deformation of the structural components during impact is required and should be representative of the real system. Such deformation can be measured for a DJI Phantom III model in a form of joint displacement with a restraining force which is represented by a force–displacement curve (or moment–angular displacement curve for rotational joint) as shown in Figure 4.

To implement these restraint characteristics in the MBS model of DJI Phantom III, the obtained curves are divided into three curves, namely, loading, hysteresis and unloading curves. These restraint characteristics were obtained from compressive quasi-static tests on the real system, as shown in Figure 3. Structural members that represent each joint were loaded (at 5 mm/s loading speed) until the structure failed or the maximum structural strength was reached. Then, the structure was unloaded at the same rate to obtain unloading characteristics.

Based on the sensitivity analysis, damping coefficient of Kelvin restraint of Joint 1 and Cardan restraint of Joints 3–6 has a significant effect on energy transfer of the system. Structural damping coefficient, c, of the kelvin restraint can be approximated using the equation:

$$c = 4\pi f \zeta m. \tag{1}$$

The natural frequency of a structure was obtained from a ground vibration test (GVT) on specific joints, having the value of 631.7 Hz and 84.5 Hz for Joint 1 and Joints 3–6, respectively. The structure of the camera gimbal is made from aluminium with multiple joints and has a damping ratio of 0.07 based on literature [18]. For the motor arm, ABS plastic material was used and the typical damping ratio of 0.05 was used. The calculated damping for Joint 1 and Joints 3–6 are 85 N s/m and 0.23 N m s/rad, respectively.

2.4. MBS models of human body and crash dummy

Figure 5(a) shows the human body model that is available in MADYMO and selected to simulate a crash test with the MBS model of the DJI Phantom III UAS. The human body model was distributed with MADYMO 7.7 (filename: h_occ50fc, version 5.2) and was published by Happee et al. [19,20]. This facet occupant model is a representative model to the real mid-sized (50th Percentile) male human body [21]. This human body model produces a more similar response to the real human body because it has a higher bio-fidelity and better compliance with a real human body

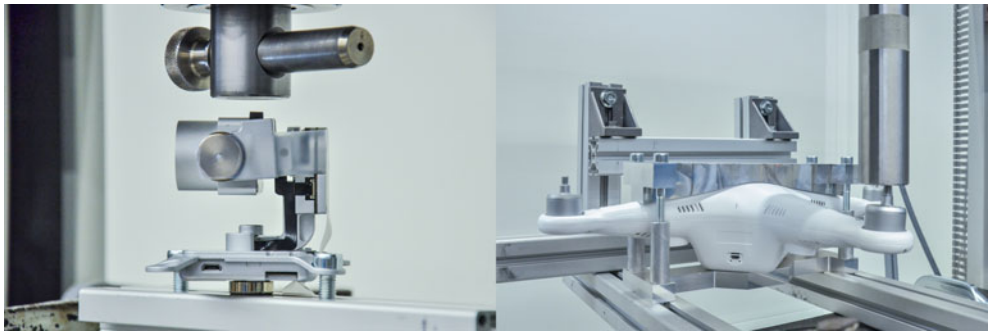

Figure 3. Examples of the experimental setup for compressive static test on UAS structural members to determine joint restraint characteristics curves for Joint 1 (left) and Joint 3 (right).

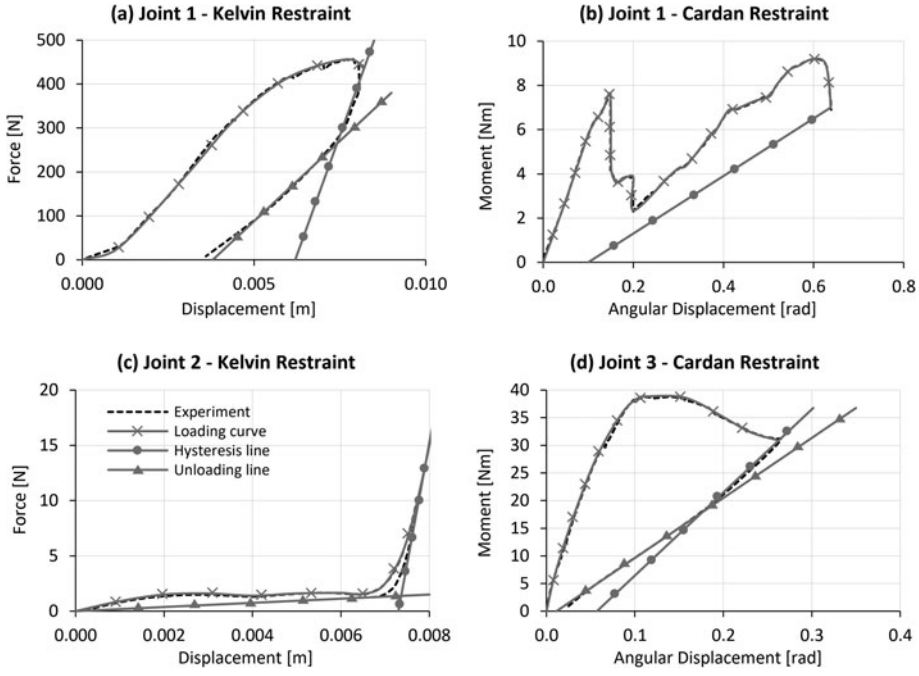

Figure 4. Example of restraints characteristics measured during experiments (black dotted line) and approximated curves for loading, hysteresis and unloading for joint 1–3. Simplified loading, hysteresis and unloading curves are used in the MBS model of the DJI Phantom III UAS.

than the Hybrid III crash dummy model that is shown in Figure 5(b).

For validation purposes, the Hybrid III crash dummy model, shown in Figure 5(b), was also integrated with the MBS model of the DJI Phantom III UAS. This Hybrid III crash dummy was also distributed with MADYMO 7.7 (filename: d_hyb350el_Q, version 2.0) [22].

2.5. Contact model

Contact between the crash dummy and the UAS was modelled based on a non-smooth, force-penetration contact model in which the contact force is a function of the penetration and velocity of penetration [14]. Contacts compliance characteristics between a UAS model and the crash dummy was approximated using an elastic-perfectly plastic contact model based on Hertz elastic contact model proposed by Brake [23]. Materials property of UAS (e.g. ABS plastic and Aluminium) was obtained from an online source, MATBASE [24]. For a crash dummy, the head contact surface was assumed to have characteristics of a human head scalp and the materials property was obtained from the experiment presented by Lozano-Mínguez et al. [25]. Since the materials properties come in ranges of values, the contact curves derived then consist of an upper and lower bound curve, corresponding to the lower and upper values of the materials properties. Additionally, the friction coefficient was introduced to contact models between the UAS and the dummy head. The friction coefficient of 0.3 was used for UAS front contact and camera bottom surface contact. To account for the dig-in effect of the camera frontal contact which has a small contact area, the friction coefficient of 1.2 was used.

In addition to the contact with the human head, two contacts between internal parts of the UAS are also accounted for. The first contact is between a damp plate and the main UAS body and the second contact is between the lower and upper parts of the camera gimbal. All contact points are presented in Figure 6. The contact compliance curves for UAS to human head contact and UAS internal parts contacts implemented in MADYMO are shown in Figure 7.

3. Validation of MBS model

The MBS model of the DJI Phantom III UAS was implemented and integrated with the human body and crash dummy models in MADYMO 7.7. Subsequently, this integrated model was validated using experimental data from a full-scale crash test between a DJI Phantom III UAS and the FAA Hybrid III crash dummy performed by ASSURE [6]. The tests measured the head centre of gravity (CG) accelerations, neck forces and moments of the crash dummy at various impact angles and velocities to estimate head and neck injuries.

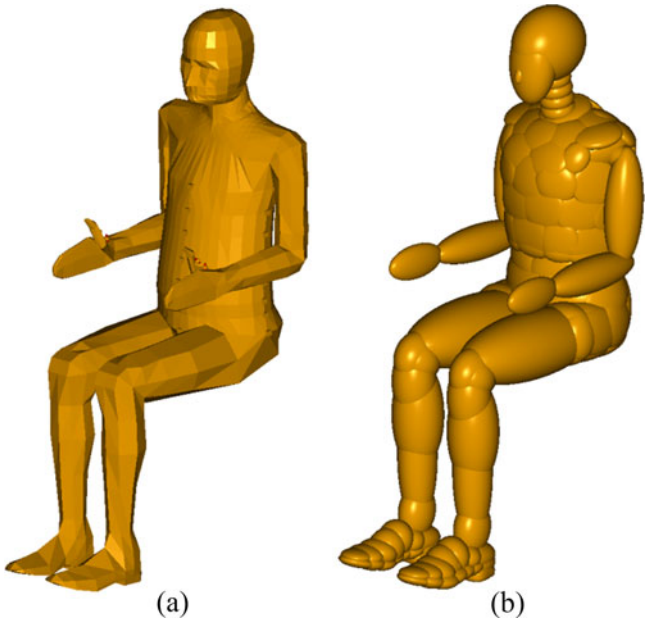

Figure 5. MBS models of human body and crash dummy: (a) Human body model from MADYMO 7.7 and (b) Hybrid III crash dummy model from MADYMO 7.7.

To ensure that the UAS model has a realistic impact force transfer to the head, head CG resultant acceleration and upper neck force of the crash dummy were validated. A simulation, which consisted of the UAS model and the Hybrid III crash dummy model, was set up in a similar manner to the ASSURE's impact tests as shown in Figure 8. The crash dummy was seated on a rigid seat with full back support and the UAS impact velocity vector was aligned towards the head centre of gravity to simulate CG–CG impact. UAS angle of attack was set at zero, aligning with the horizontal axis. Elevation angle, θ, and impact velocity, V_{impact}, of the UAS model was set to simulate equivalent testing conditions to the ASSURE experiments. Three impact cases that were validated were vertical, angle and horizontal impact cases, which correspond to θ of 90°, 58°/65° and 0°, respectively. The simulation was run on a 2.6 GHz processor, resulting in a computational time for each simulation of approximately 120 s.

3.1. Vertical impact validation

For vertical impact case ($\theta = 90°$) in which the UAS model fell vertically on the crash dummy, validation was performed at two impact velocity: 9.9 m/s and 15.1 m/s. Figure 9 shows

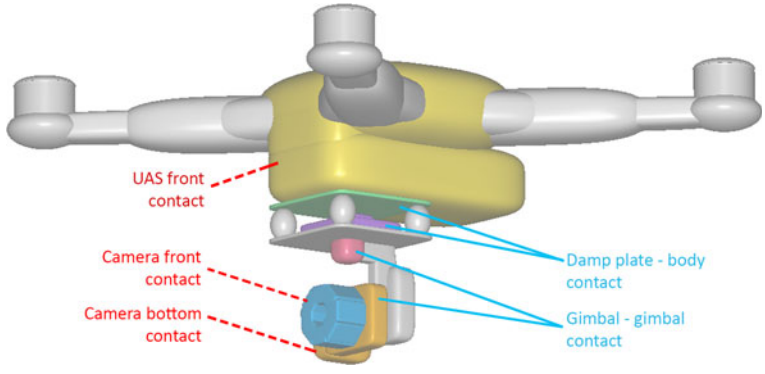

Figure 6. Illustration of contact areas between UAS and crash dummy head (dotted line) and contact areas of UAS internal parts (solid line).

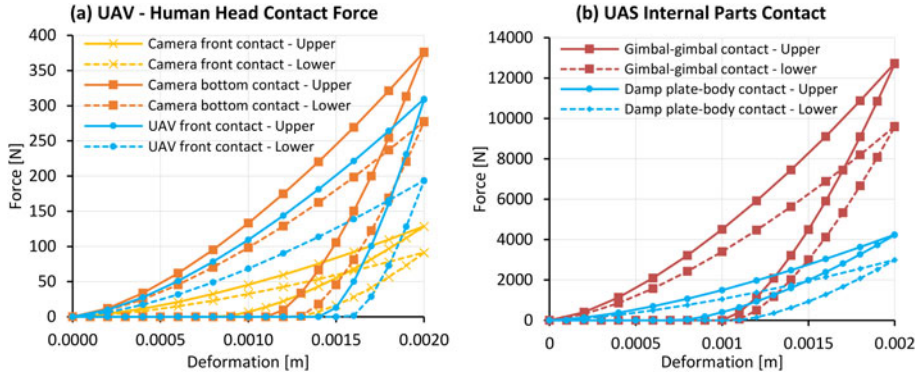

Figure 7. Contact compliance curves for (a) UAV – human head contacts and (b) UAS internal parts contacts derived using an elastic–perfectly plastic contact model based on Hertz contact proposed by Brake [23].

a comparison of time sequences between the model and the test of the vertical impact event at 15.1 m/s impact velocity. The kinematic of the UAS model corresponds well with the experiment, showing similar full compression phase of the UAS at approximately 7 ms, and similar rebound and rotational characteristics.

Figure 10 shows a comparison of head CG resultant acceleration in the time domain of the vertical impact case at 9.9 m/s and 15.1 m/s between the model and ASSURE's experiment. For impact velocity of 9.9 m/s, the simulated results show a good correlation with Experiment 2 but show slight discrepancy with Experiments 1 and 3. Despite the differences in experimental results, it is obvious that the simulated model can produce a very similar trend to the real-world system. For 15.1 m/s, the acceleration from the model agrees well with the experimental results for the first 5 ms. In the figure, the first peak represents the contact force from the contact initiation between the two bodies. The second peak occurs when the whole UAS body transfers impact energy to the dummy head, while the third peak shows the UAS bouncing off the dummy head. The primary first and second peak corresponds well with the real system, while the third peak shows a significant difference. In the third peak region, the head acceleration from the model damps out at a slower rate compared to the experimental results. It is influenced by two main factors: rebound characteristics of the UAS model and the dummy model neck response.

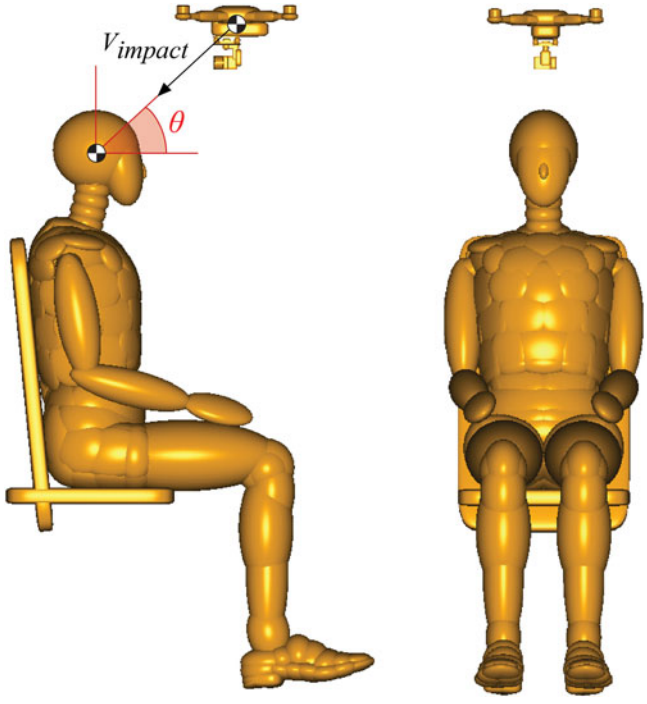

Figure 8. Setup for integrated model validation in MADYMO. The MBS model of the Hybrid III 50th percentile (male) crash dummy that was used in ASSURE impact drop testing [6]. For the model, the dummy is assumed to be seated on a rigid seat and the UAS impact velocity is aligned with the CG of the crash dummy.

The accuracy of the model of such a complex system typically deteriorates over time, as more components are interacting and influencing one another. In addition, such discrepancy between the model and experiments may come from the lack of damping introduced in the model – these parameters are difficult to measure and model accurately. Nevertheless, for such impact case, the first two peaks are most important to the determination of the head injury criteria, such as the HIC_{15}.

Upper neck force in x- and z-directions was validated for vertical impact at 9.9 m/s and 15.1 m/s impact velocity as shown in Figure 11. For the upper neck force in the x-direction, the model over predicts the maximum peak force by approximately 60% and 33% for 9.9 m/s and 15.1 m/s, respectively. Despite the large percentage differences, the force differences, which are less than 100 N, are not large enough to significantly affect neck injury

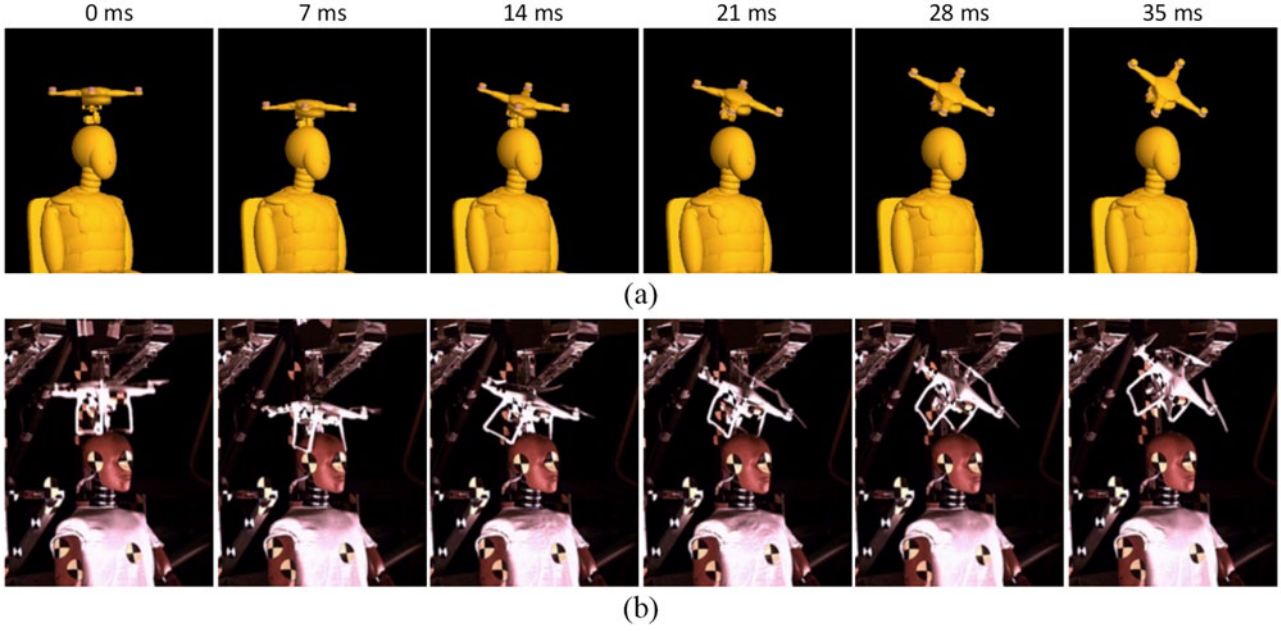

Figure 9. Comparison of (a) MBS model versus (b) ASSURE experiment from [17] at 90° elevation angle and 11.2 m/s impact velocity.

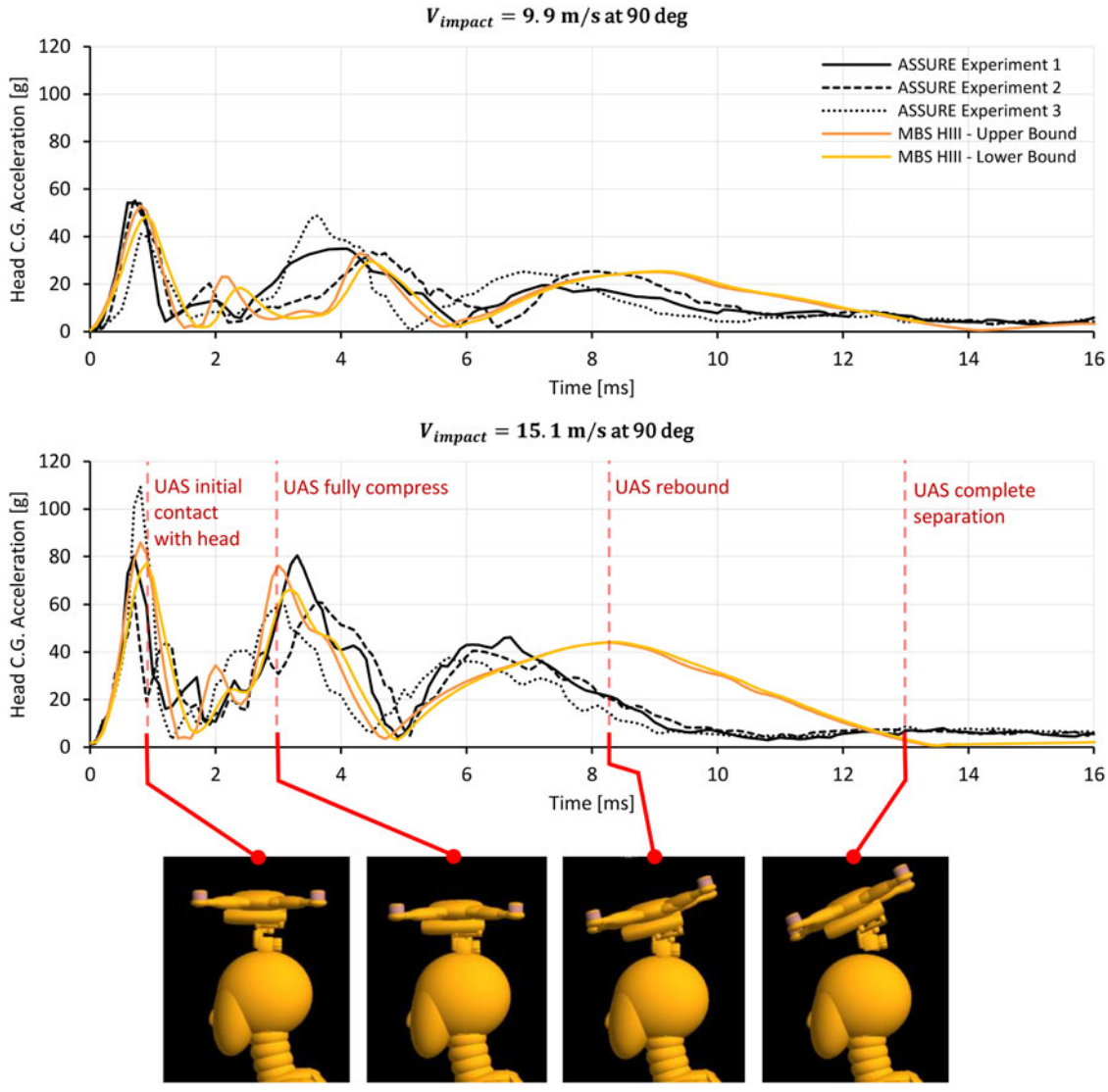

Figure 10. Comparison of the resultant acceleration–time history of head CG between MBS model and ASSURE experimental results at 9.9 m/s and 15.1 m/s impact velocity and 90° impact angle.

prediction. Furthermore, upper neck force in the *z*-direction for both velocities from the model show good agreement with the experiments with approximately 13% and 6% differences in peak force values for 9.9 m/s and 15.1 m/s, respectively.

3.2. Angled impact validation

Head CG accelerations and upper neck forces were validated at impact angles of 59° and 65°. Figure 12 shows a comparison of time sequences between the model and experiment of 65° impact event at 11.3 m/s impact velocity. The overall kinematics of the UAS model is different from the experiment. Such differences can be explained by the differences in the UAS model fidelity. In this angle impact, camera-gimbal which is the contact point is modelled as a single lumped mass with only a translational and revolute joint. Such a simplified model differs from the real UAS which consists of multiple revolute joints and free-rotating parts, thus leading to the differences in the timing of parts interaction. In addition, the camera points forward in the model, while in the experiment, the camera pointed downward – resulting in different moment arm lengths.

In Figure 13, the model produces similar trends for head CG accelerations compared to the tests. The contact force and its damping characteristics of the model produces an over-estimated head acceleration as can be seen in the variations of the first peak. One of the influencing factors is contact damping, which is not introduced in the contact model. In the real system, skin damping is expected as the crash dummy skin is made of vinyl which is highly damped. In addition, the full compression phase of the UAS in the test (represented by the second peak of the head acceleration) occurs approximately 2 ms after the contact phase. Such lagging is different from the model because the model does not include the effect of free rotating parts and has a lower number of joints.

For upper neck forces in *x*- and *z*-directions, the model corresponds well with the tests but with a slight overestimation of the contact forces, which are shown at

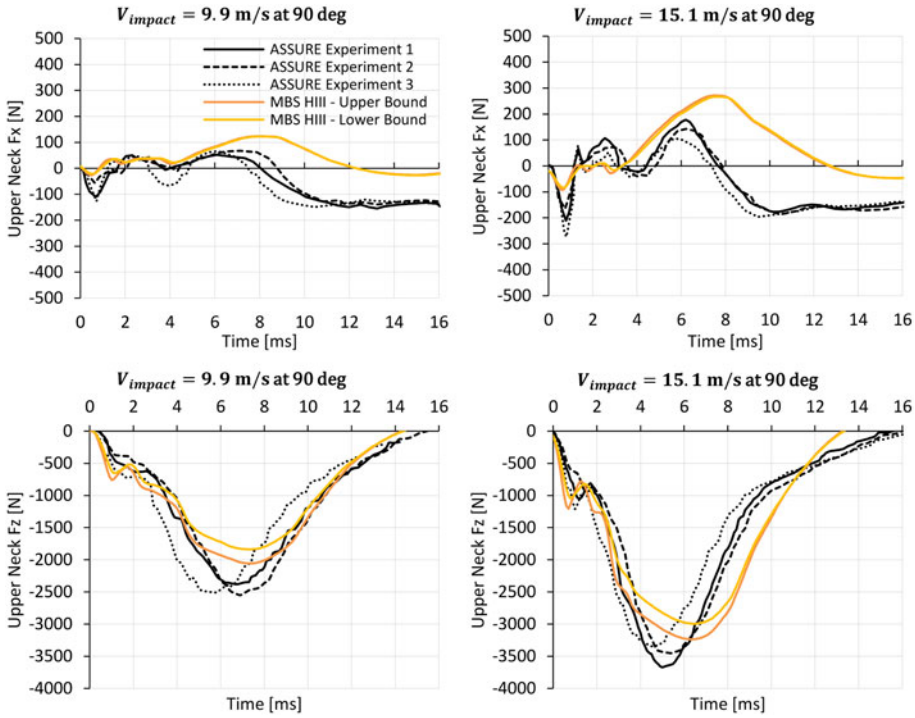

Figure 11. Comparison of force–time history from the upper neck load cell in *x*- and *z*-directions between MBS model and ASSURE experimental results at impact velocities of 9.9 m/s and 15.1 m/s and at 90° elevation angle.

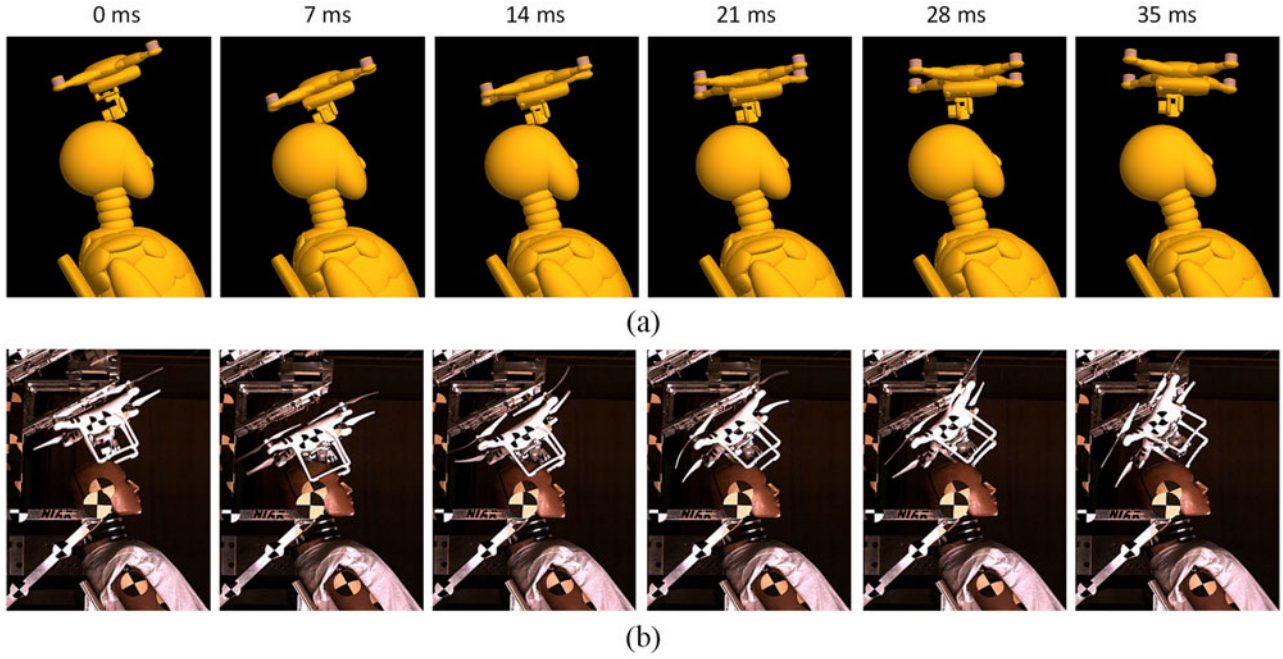

Figure 12. Comparison of (a) MBS model versus (b) ASSURE experiment from Ref. [17] at 65° elevation angle and 11.3 m/s impact velocity.

approximately 1.5 ms in Figure 14. The peak force differences for 14 m/s at 58° impact case is less than 10%. For 11.2 m/s at 65° impact case, the peak force differences are within 15%, which is within an acceptable limit of 20%.

3.3. Horizontal impact validation

The horizontal impact was the last validation case, in which head CG accelerations and upper neck forces were validated. Figure 15 shows the comparison for head CG accelerations between the model and the tests. The modelling result corresponds well with Experiment 2 (with 4% difference in peak acceleration) but shows a significant difference to Experiments 1 and 3. Nevertheless, there is a large discrepancy between the experimental results. In horizontal impact case, a full-body collision occurs, meaning that only a centre mass of the UAS mainframe contacted the dummy head. No other components, such as camera gimbal, in between

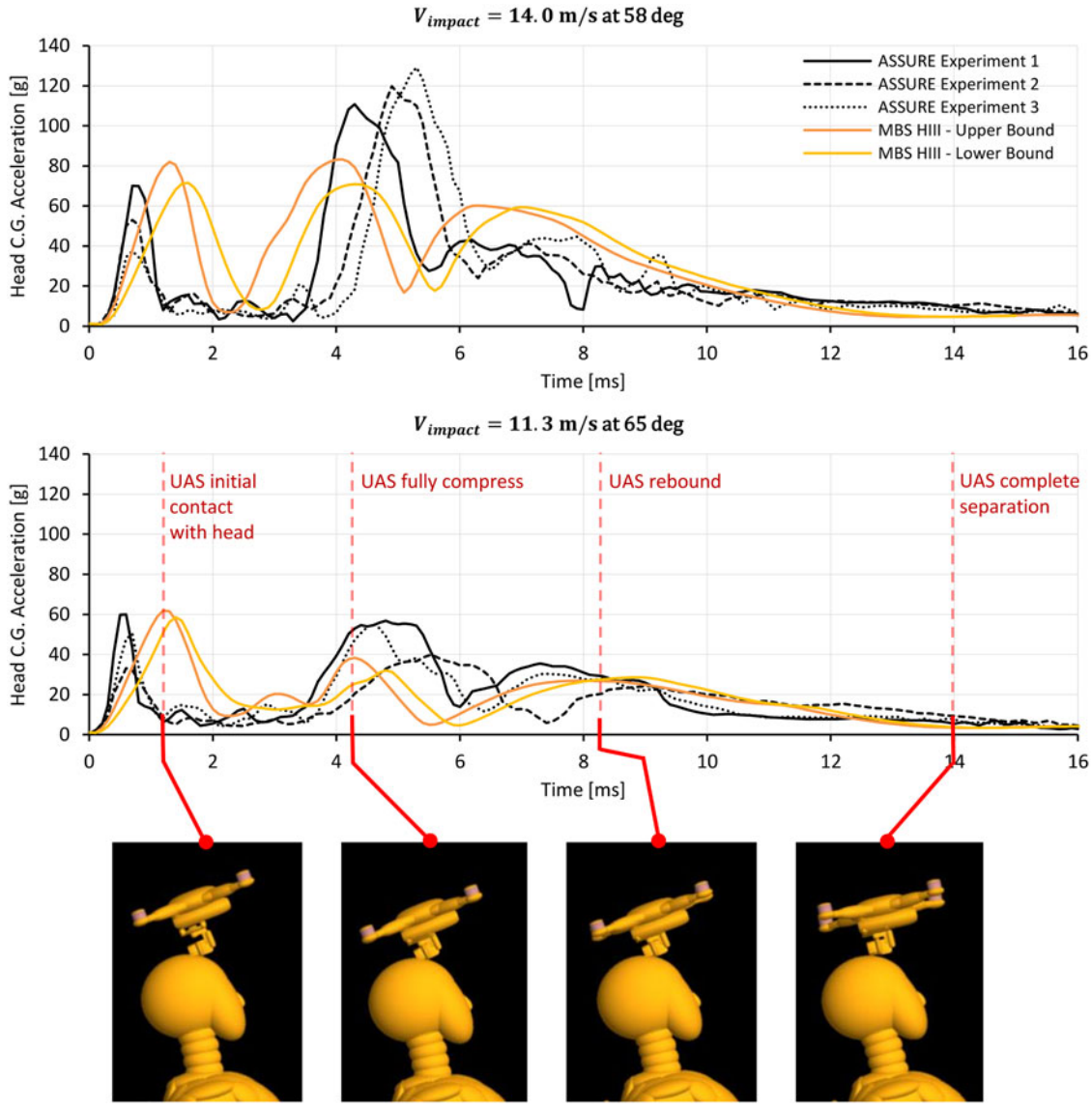

Figure 13. Comparison of resultant head CG acceleration–time history between the MBS model and ASSURE experimental results. Impact velocities of 11.3 m/s and 14.0 m/s at 65° and 58° impact angle, respectively.

to delay impact time. Thus, only a single peak of head CG acceleration is observed.

For upper neck forces shown in Figure 16, the model produces similar trends compared to the tests for both *x*- and *z*-directions but with different peak force magnitude. For the force in the *x*-direction, the model peak force difference compared to Experiment 2 was almost 58%. The model peak force difference reached almost 74% for the force in the *z*-direction compared to Experiment 2. In the experimental results, upper neck force in *z*-direction almost doubled the force in the *x*-direction, which is opposite to the modelling results where the force in *x*-direction doubled the force in the *z*-direction. The differences may stem from the contact point which may differ between the model and the tests, and MADYMO crash dummy's simplified facial details which were represented by only a smooth ellipsoid without a nose. Additionally, the gravitational effect was not included in the model, which may give a downward velocity to the UAS upon impact.

3.4. Head injury criteria levels

Based on the validated head CG acceleration and neck forces/moments results from the model, the head injury criteria (HIC) and neck injury criteria (N_{ij}) were computed and compared against the experimental results. For the HIC injury criteria, HIC_{15} was implemented as it is suitable for short duration impact (The value 15 refers to the 15 ms time period starting from the moment of impact). Functionally, the HIC represents the peak average power delivered to the head [26]. Based on Federal Motor Vehicle Safety Standards (FMVSS), a HIC_{15} value of 700 is considered to be a minimum safety standard for non-fatal impact [27]. The equations for the HIC is

$$\mathrm{HIC} = \max\left[\frac{1}{t_2 - t_1}\int_{t_1}^{t_2} a(t)dt\right]^{2.5}(t_2 - t_1). \qquad (2)$$

Proposed by the National Highway Traffic Safety Administration (NHTSA), the N_{ij} is a neck injury criterion

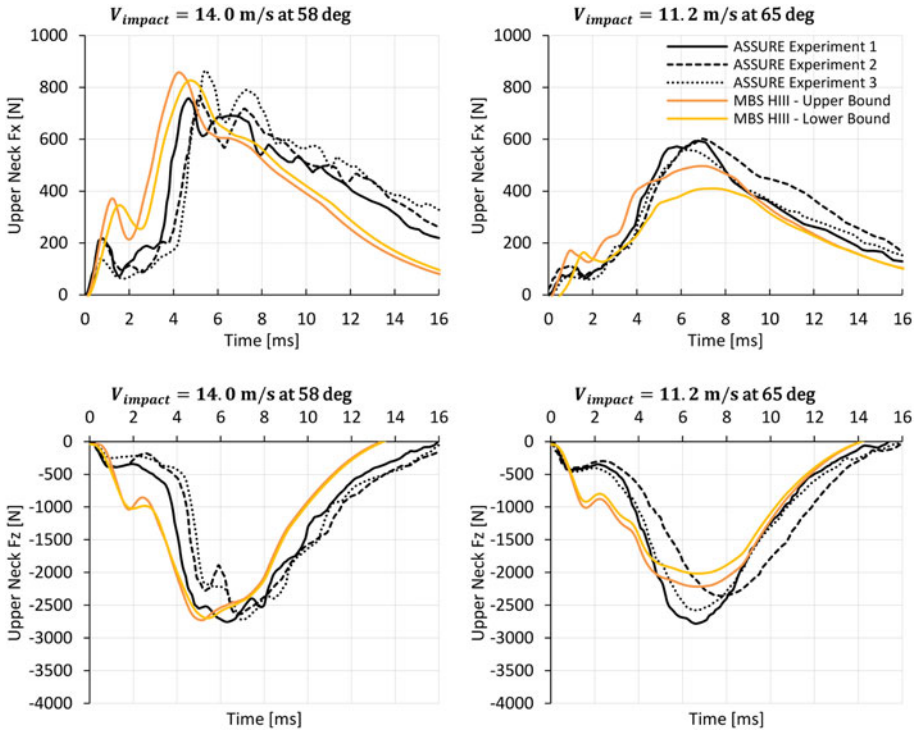

Figure 14. Comparison of the force–time history of angle-impact cases of the upper neck load cell in *x*- and *z*-directions between MBS model and ASSURE experimental results. Impact velocities of 11.3 m/s and 14.0 m/s at 65° and 58° impact angle, respectively.

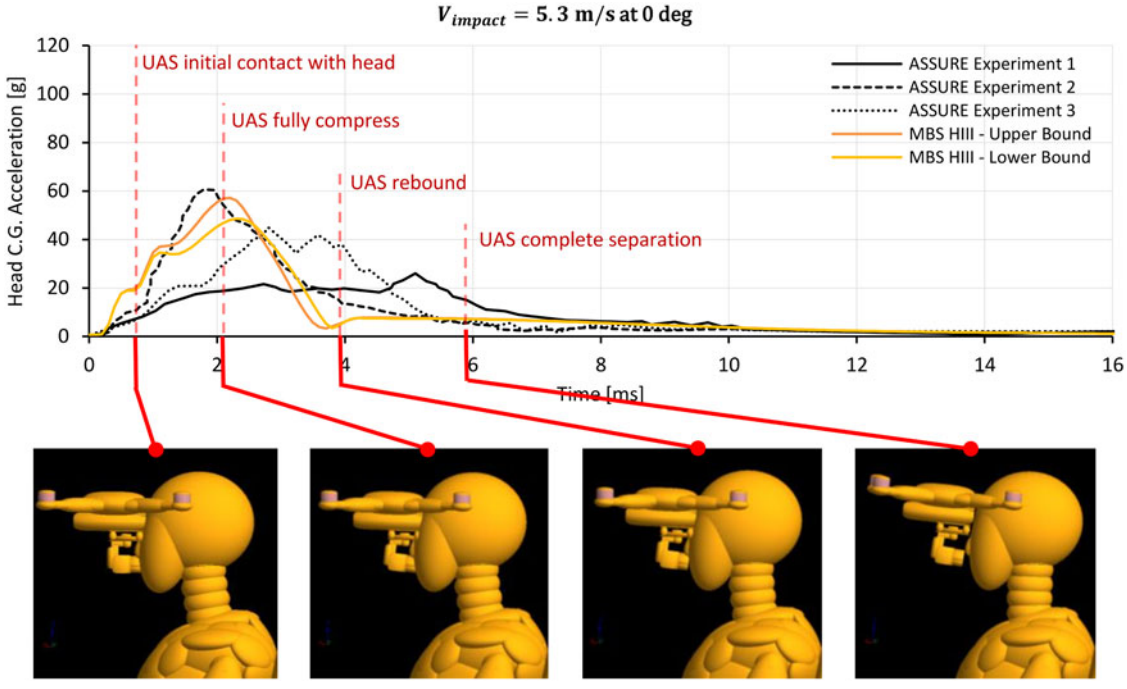

Figure 15. Comparison of resultant head CG acceleration–time history between the MBS model and ASSURE experimental results. Impact velocity of 5.3 m/s at 0° impact angle.

which considers the upper neck force and moment [28]. The '*ij*' represents indices for the four injury mechanisms; namely N_{TE}, N_{TF}, N_{CE} and N_{CF}. The first index represents the actual load (tension or compression) while the second represents sagittal plane bending moment (neck flexion or extension). The current performance limit of the N_{ij} is 1 which represents a 22% risk greater than the Abbreviated Injury Scale (AIS) level 3 [29]. The equation for the N_{ij} is

$$N_{ij} = |\frac{F_z}{F_{\text{int}}}| + |\frac{M_Y}{M_{\text{int}}}|, \tag{3}$$

where F_z is the axial load, F_{int} is the corresponding critical intercept value of load, M_Y is the flexion/extension bending moment computed at the occipital condyles (OC) and M_{int} is the corresponding critical intercept value for moment [27]. Using the equations above, the values for HIC_{15} and

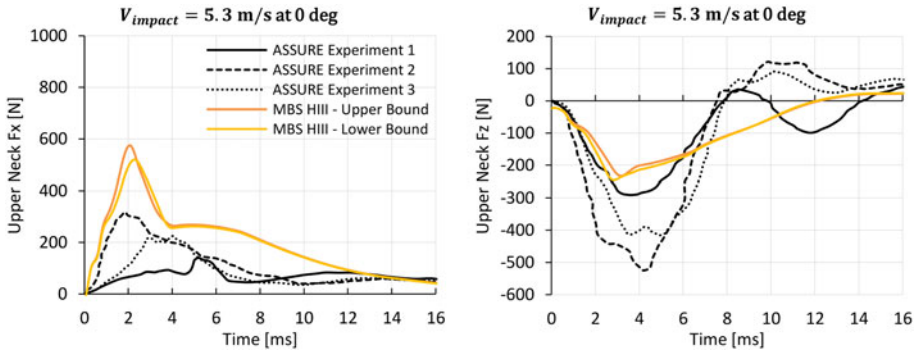

Figure 16. Comparison of the force–time history of angle-impact cases of the upper neck load cell in *x*- and *z*-directions between MBS model and ASSURE experimental results. Impact velocity of 5.3 m/s at 0° impact angle.

Table 4. Comparison of HIC_{15} and N_{ij} between MADYMO simulation (average values) and experimental results.

Impact Angle [°]	Impact Velocity [m/s]	MADYMO				
		HIC_{15}	$N_{ij}-N_{TE}$	$N_{ij}-N_{TF}$	$N_{ij}-N_{CE}$	$N_{ij}-N_{CF}$
90	9.9	14.0	0.101	0.000	0.402	0.008
	15.1	63.3	0.087	0.028	0.659	0.108
65	11.3	26.5	0.079	0.059	0.095	0.330
58	14	132.1	0.123	0.089	0.136	0.518
0	5.3	24.8	0.080	0.010	0.039	0.055
Impact Angle [°]	Impact Velocity [m/s]	Experiment				
		HIC_{15}	$N_{ij}-N_{TE}$	$N_{ij}-N_{TF}$	$N_{ij}-N_{CE}$	$N_{ij}-N_{CF}$
90	9.9	14.2 ± 2	0.117 ± 0.006	0.040 ± 0.000	0.447 ± 0.025	0.050 ± 0.000
	15.1	49.9 ± 8	0.097 ± 0.006	0.050 ± 0.000	0.633 ± 0.015	0.167 ± 0.202
65	11.3	28.6 ± 10	0.063 ± 0.006	0.077 ± 0.006	0.073 ± 0.006	0.520 ± 0.010
58	14	125 ± 20	0.090 ± 0.010	0.093 ± 0.006	0.090 ± 0.010	0.517 ± 0.015
0	5.3	24.36 ± 5	0.067 ± 0.006	0.010 ± 0.010	0.060 ± 0.044	0.047 ± 0.046

Colour scale shows percentage difference level, ranging from percentage difference interval of 0–10% (light grey), 10–20% (grey), 20–30% (dark grey) and ≥30% (black).

N_{ij} from the model were calculated and compared against the experimental results as shown in Table 4.

Based on the comparison in Table 4, the HIC_{15} from the model correlates well (differences less than 10%) with the experimental results, except for 90° impact case at 15.1 m/s (difference of 20–30%). For the N_{ij} injuries prediction, the model estimated comparable values to the experimental results. Even though the upper neck force influences the N_{ij} levels, the upper neck moment is also critical. Upper neck moment is sensitive to impact positions, seating postures of the dummy, as well as dummy's neck positions and angles. Therefore, the upper neck moment is one of the contributing factors to this discrepancy. It should also be noted that the N_{ij} levels that exceeded 30% difference from the experimental data are mostly of low values that are not significant. Despite slight discrepancies, the comparison that the UAS model simulating a similar impact response and can produce a realistic head and neck injuries.

4. UAS impact on the human body

Applications of UAS operations may pose ground collisions risks to human. With the validated UAS multi-body system models, impact severity on the human body due to UAS collision can be simulated and analysed. Figure 17 shows an impact simulation setup between the UAS model and the human body model in MADYMO. The objective of the simulation is to determine the head (HIC_{15}) and neck (N_{ij}) injuries of the human body due to UAS collisions.

The simulation was performed on frontal, side and rear impact (corresponding to the impact angle, α, of 0°, 90° and 180°, respectively) at various elevation angles, θ. Impact velocities, V_{impact}, were varied from 0 to 18 m/s with an

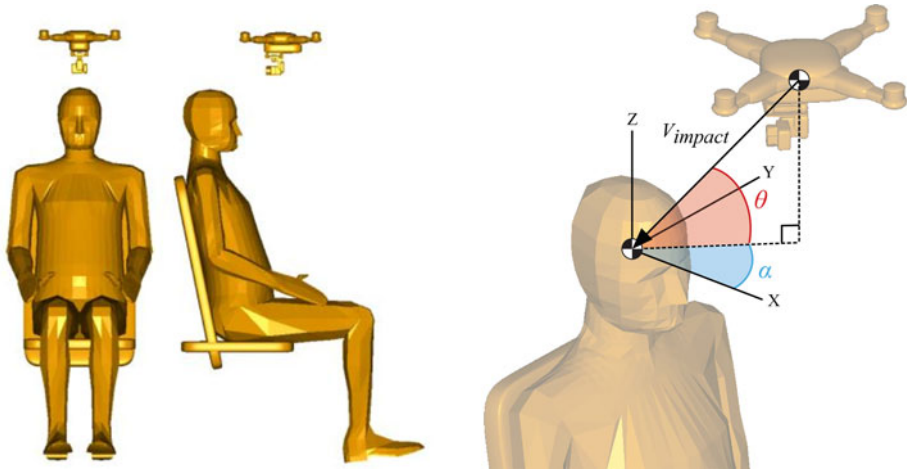

Figure 17. UAS to human body model impact setup in MADYMO. α is the impact angle on the transverse plane in which 0°, 90°, 180° correspond to frontal, side and rear impacts, respectively. θ is the elevation angle in which 0°, 45° and 90° correspond to horizontal, angle and vertical impacts, respectively.

increment of 2 m/s. The human body model was seated on a non-smooth rigid seat with contact definition predefined by MADYMO. An impact velocity vector from the UAS CG was aligned towards human body head CG in order to simulate CG to CG impact conditions. The UAS angle of attack was fixed to 0° from the horizon axis for all impact case. By solving the model on a 2.6 GHz processor, the computational time for each simulation took approximately 30–40 s.

4.1. Head injury criteria

From the simulations, the HIC_{15} for frontal, side and rear impact were calculated and plotted in Figure 18. The maximum operational speed for the DJI Phantom III is 16 m/s and is overlaid in the figure to specify the limit. From the figure, the value of HIC_{15} rises non-linearly as impact velocity increases, while the slope increases as the elevation angle increases for frontal, side and rear impact.

For frontal impact ($\alpha = 0°$), the HIC_{15} exceeds the specified limit of 700 at approximately 14.8 m/s at 0° elevation angle which corresponds to the horizontal impact. At the UAS maximum speed of 16 m/s, the HIC_{15} already passes the value of 903, in which a risk of serious head injury is probable. The elevation angle of more than 20° results in the HIC_{15} level of less than 700. For side impact, the HIC_{15} value exceeds 700 at approximately 15.5 m/s for the elevation angles of 0°, 10° and 20°. At the maximum speed of 16 m/s, the maximum HIC_{15} value reaches 797 for 20° elevation angle. As for rear impact ($\alpha = 0°$), the HIC_{15} value passes 700 at 14 m/s and 14.5 m/s for the elevation angles of 0° and 10°, respectively. For 0° elevation angle at rear impact, as the UAS reaches maximum speed, the HIC_{15} exceeds the value of 1000.

It is evident that the HIC_{15} value decreases as the elevation angle increases. For all three impact angles, severe head injury is less probable as the elevation angle goes beyond 30°. For all impact angles, the elevation angle of 90° (vertical impact) results in less than 200 of the HIC_{15} value at the maximum UAS velocity.

4.2. Neck injury criteria (N_{ij})

The N_{ij} results from the simulations are plotted in Figures 19–21. For all impact angles (frontal, side and rear), N_{TE} and N_{TF} values are relatively low compared to N_{CE} and N_{CF} since the applied load often results in compression and rotation of the human neck. For all impact angles, the N_{CE} and N_{CF} values increase as the impact velocity increases and the slope of the curves rises as the elevation angle increases. Higher elevation angle means that the load direction of the UAS on the head becomes more vertical, resulting in a larger compressive force in the neck. It is evident that serious neck injury due to the DJI Phantom III UAS ($w_0 \approx 1.2$ kg) collision is improbable to occur to the human body, as the N_{ij} values are less than 1 for all impact and elevation angles.

For frontal impact case, the neck injury is most likely to occur under vertical and angle load cases ($\theta > 60°$) due to a higher compressive load in the neck. Horizontal impact case ($\theta \approx 0°$) is less likely to inflict any neck injury which is in contrary to the head injury. Like the side impact case in which compressive load is more prominent than the flexion/extension upper neck moment, the neck injury is also low for horizontal impact case. The N_{ij} results for side impact case is shown in Figure 20.

Rear impact, which is quite different from the frontal impact case, shows that neck injury is most likely to occur at elevation angle, θ, of 60°. As shown in the N_{CE} plot in Figure 21, the N_{CE} value reaches approximately 0.52 at the maximum UAS operational speed of 16 m/s. Since there is no frontal support for the thorax, the head, neck and upper body moved forward freely, resulting in a hyperextension of the neck. The result is a lower compressive force, but a larger extension moment in the upper neck.

In addition, Figure 22 shows the comparison of the overall trends between the N_{ij} and the HIC_{15} at different

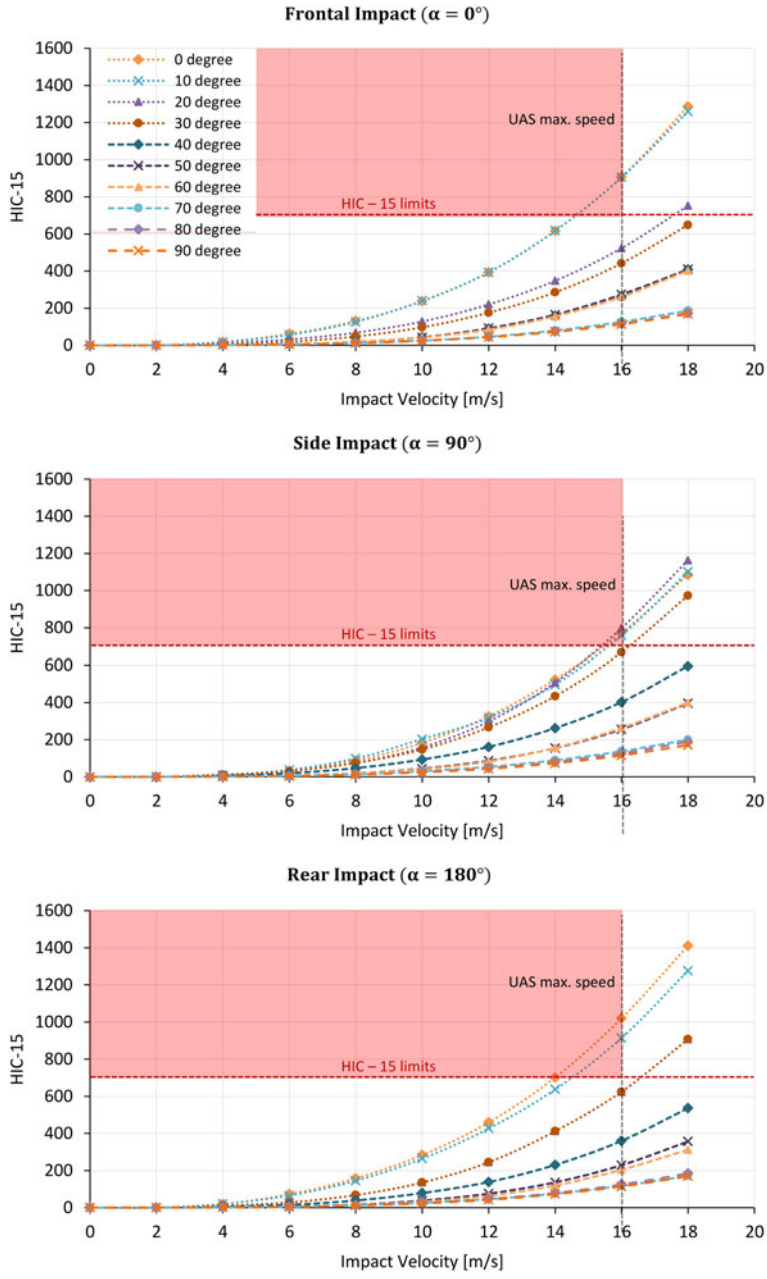

Figure 18. Calculated head injury criteria (HIC_{15}) from the UAS–human body model simulation at different impact velocities and speeds for frontal, side and rear impact cases. The value of 700 is the limits for HIC_{15} in which no critical head injury occurs.

elevation angles at UAS maximum velocity of 16 m/s. As the elevation angle increases, the N_{ij} values (such as N_{CE} and N_{CF}) increases while the HIC_{15} decreases. This shows that the loading direction plays a significant role in determining the injury mechanism. Vertical load on the human head inflicts higher neck injury more than the head injury, while horizontal load inflicts head injury more. In horizontal impact where the elevation angle is at 0°, the neck system has minimal effect in absorbing impact energy, resulting in higher head CG acceleration. As the elevation angle increases, the impact force starts to transfer directly into the neck system, lowering and increasing the chance of head and neck injury, respectively. The neck injury is highest when the elevation angle is roughly 60°–70° due to the high compressive force in the upper neck that is coupled with neck extensive/flexion moments.

5. Discussion

5.1. Discussion on UAS MBS modelling and validation results

The developed UAS MBS model shows a good correlation to the real impact experiments and can be used to simulate the ground impact on the Hybrid III crash dummy. This modelling technique allows a fast computational time when compared to FEM modelling, which is preferable if various impact cases are being investigated. A single lumped mass with a single Kelvin and Cardan springs/dampers representing a gimbal system produces results in vertical impact case similar to the experiments. However, in an angle impact case, such simplified lumped mass can only produce a similar trend of impact force transfer but need further refinement in order to better match the experimental results.

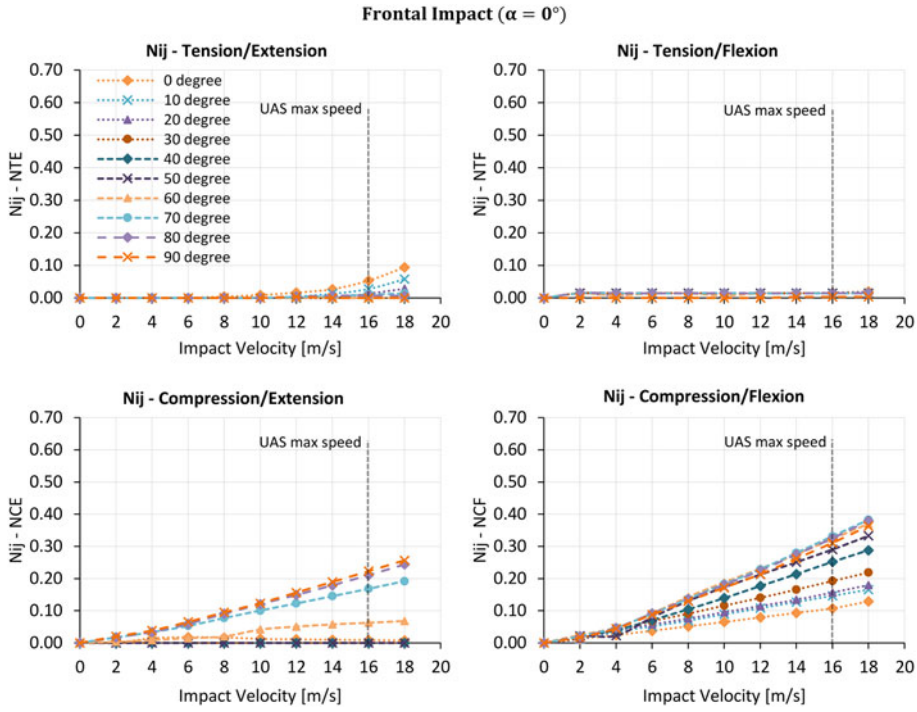

Figure 19. Calculated neck injury criteria (N_{ij}) from the UAS–human body model impact simulation at different impact velocities and elevation angles for side impact case.

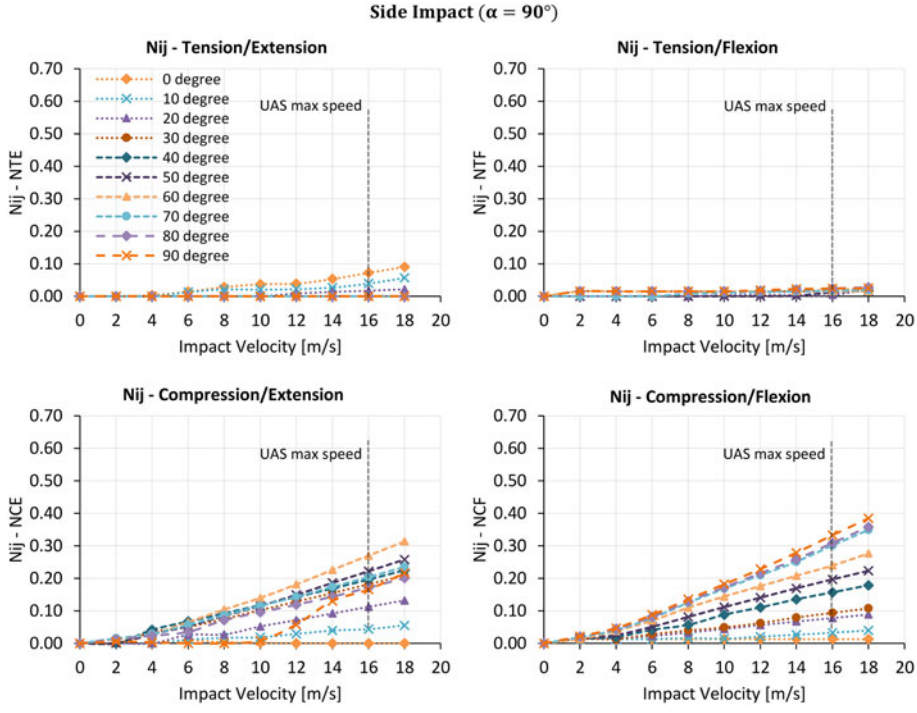

Figure 20. Neck injury criteria (N_{ij}) from the UAS–human body model impact simulation at different impact velocities and elevation angles for side impact case.

Improving it could result in a better impact response, but with a trade-off on model simplicity and computational time. Further investigation is still needed to see the value of such improvement.

The contact force characteristics derived using analytical equation gives a good response as shown in the validation results. However, contact damping was not included which is rather unrealistic since there are no materials without internal damping. The lack of damping resulted in an over-predicted contact force which is shown in Figures 13 and 14. For joint restraint characteristics, by obtaining force–deflection curves experimentally enable the non-linear effect of the real system to be captured, which can also include internal parts breakage as shown in Figure 4(b). This approach produces good results in all impact cases and resulted in realistic kinematics of the UAS.

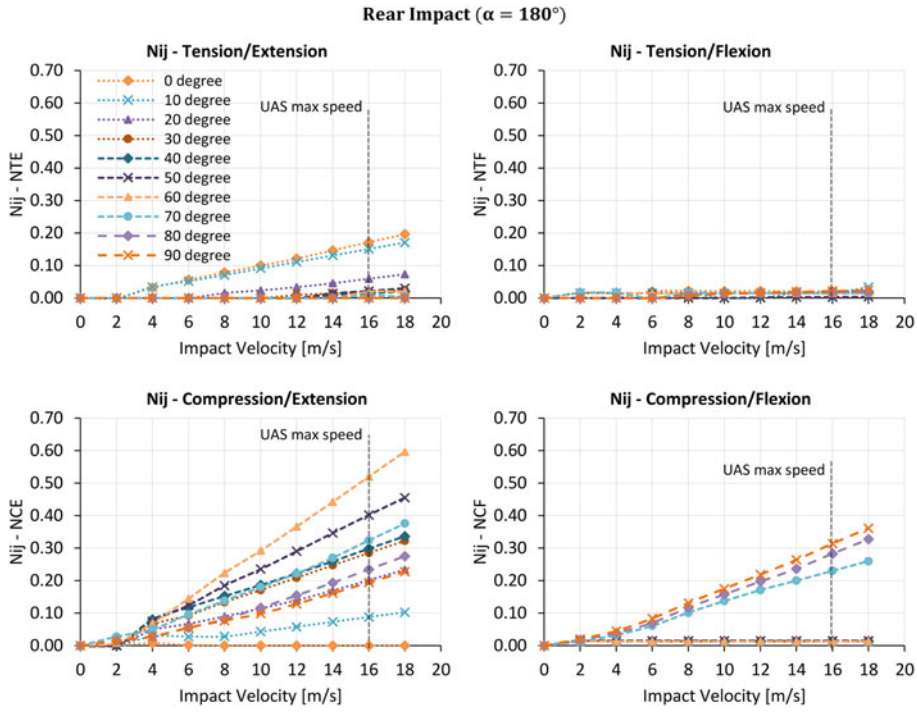

Figure 21. Neck injury criteria (N_{ij}) from the UAS–human body model impact simulation at different impact velocities and elevation angles for rear impact case.

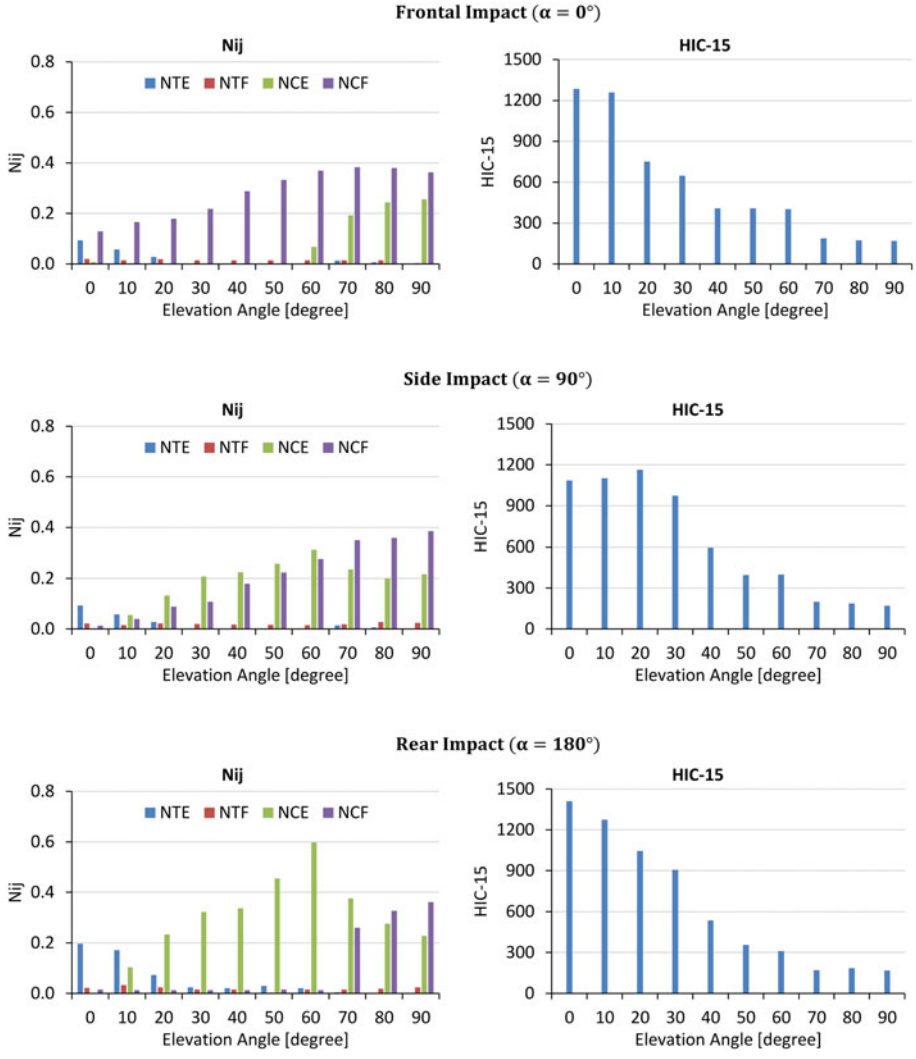

Figure 22. Analysis of elevation angle effect on the N_{ij} and HIC_{15} overall trends for frontal, side and rear impact at UAS maximum velocity of 16 m/s.

Furthermore, the estimation of the damping coefficient for joint restraints proved to be rather difficult. No simple analytical method was appropriate to use and, thus, a ground vibration test was performed for critical joint restraints to determine the natural frequencies. Using Equation 1, the damping coefficient was approximated and implemented in the model. This method resulted in good results. However, a better approximation can be done by performing a parameter estimation based on a set of calibration data. The optimisation algorithm, such as a genetic algorithm, can be employed to automatically search and estimate damping coefficients for all joint restraints. This will be considered in future work.

5.2. Discussion on human body injury, limitations and future work

According to the presented results in Section 4, a UAS poses serious harm to the human head when a full body collision (collision without gimbal in between the UAS and the human head) is expected. Such collision is seen in horizontal impact cases where elevation angle, θ, is at 0°. A gimbal system underneath the UAS significantly lessens the head/neck impact severity by absorbing the impact energy of the UAS. In vertical impact, the UAS was assumed to fall with a constant angle of attack horizontally to the ground, resulting in the gimbal hitting the human head first. Practically, it is unlikely that such a perfect collision may occur. On the other hand, a UAS would often lose balance and spin down with uncontrolled attitude. This may result in a full body collision where the main fuselage of the UAS collides on the human head and serious head/neck injury could be expected. This impact attitude variation will be further investigated in the future work to determine the worst impact attitude.

Furthermore, both the HIC_{15} and N_{ij} plots show that rear impact, which resulted in the head moving forward, inflicted higher injury than frontal and side impacts. One possible explanation is the back seat which does not support the human body in forward motion. Without such support, the head can accelerate forward easier without a significant restraining force from the neck system. This shows that for an analysis of UAS collision on pedestrian where there is no seating support, a more elaborated simulation and analysis is needed. A future work should also include a simulation setup where the pedestrian is in a standing position and walking velocity should be incorporated.

There is also quite a significant difference in HIC_{15} and N_{ij} values between a crash dummy and the human body which is expected. Even though crash dummies are based on the human body, road vehicle crashworthiness analysis shows that limitations in biofidelity of the dummies can result in different biomechanical head and neck responses compared to the real human [30]. Based on the work by Sances and Kumaresan [31], an experimental work comparing between the Hybrid III crash dummy and human cadaver under an inverted drop showed that the dummy neck was two to four times stiffer than human cadavers. Additionally, a follow-on experiment by Sances et al. [32] indicated that the crash dummy system transmits about 70–75% of the applied force from the head or upper neck to the lower neck area. On the other hand, only about 20–30% of the applied force was transmitted from the head to the lower neck in the study on a human cadaver. Future work will elaborate on such difference to understand if an appropriate UAS weight threshold can be made based on a crash dummy.

In this article, only a few injury criterions were used to investigate injury on the human body, namely, head injury criterion (HIC15) and neck injury criterion (N_{ij}). HIC_{15} is quite suitable for the problem investigated but other head injury criteria should also be employed, such as, brain injury criterion (BrIC) which considers head rotational acceleration [33]. N_{ij} was implemented in this work to investigate neck injury, but this criterion is mainly designed for whiplash injury analysis which only considers injury in flexion/extension directions. Thus, N_{ij} is not appropriate for side impact analysis and other neck injury criteria will be further investigated in future works, namely; N_{km}, NIC, LNL or ND criteria. For example, N_{km} considers the side force in the upper neck, making it more appropriate for side impact case. Therefore, the neck injury analysis in this work needs further elaboration before a sound conclusion can be made on the human neck injury level due to UAS collision.

Lastly, one of the main advantages of employing a MBS approach to model such collision scenarios is the scalability of the model. With a simplified model construct, this allows the UAS model to be scaled up or down in terms of size and mass. Scaling factors will need to be determined experimentally for each joint restraint characteristics, damping coefficients and mass/inertia properties. This scalability of the model will be included in future work.

6. Conclusions

In this article, a MBS model of a DJI Phantom III UAS was developed and integrated with a validated human body and crash dummy models that are available in MADYMO. The DJI Phantom III represents a small UAS weight class ($w_0 \approx 1.2$ kg). The developed MBS consists of multiple lumped masses which are connected via restraint joints. Each joint is restrained using Kelvin spring and damper, and force–deflection characteristics of each joint were obtained experimentally. Force penetration contact model, derived analytically, was implemented to model impact interaction between the UAS and a crash dummy (or the human body), as well as interactions between the UAS internal parts.

The integrated model of DJI Phantom III UAS contacting and impacting the crash dummy has been validated by comparing model simulation results with ASSURE experimental results of DJI Phantom III UAS drop tests on a Hybrid III crash dummy. This comparison shows that the simulated impact events and impact forces are similar to those measured in the real-world impact tests of ASSURE, at various impact velocities and elevation angles.

Using the validated UAS model, impact simulation of the UAS collision on the human body was performed. The aim was to determine the impact severity of the UAS on the human body. Frontal, side and rear impacts were

investigated, and the elevation angles were varied to simulate horizontal, angle and vertical impact cases. Based on the head injury criterion (HIC_{15}), the results show that UAS horizontal impact can inflict HIC_{15} of more than 700. This means that serious head injury, such as skull fracture or brain damage, is probable. For neck injury, the prediction N_{ij} criterion shows that there is a low chance of neck injury and vertical impact tends to inflict higher neck injury, but still within the N_{ij} performance limits of 1. Therefore, based on the analysis in this paper, it can be concluded that the UAS with a mass of approximately 1.2 kg can inflict serious head injury on the human body.

Follow-up research will be to extend the MBS model development and integration with human body models in MADYMO for other UAS types and for other human body models than the 50% male one. With the extension to other UAS types, the effect of landing gears will be included for offset impact analysis on the human head.

Acknowledgments

The authors would like to thank Delft Aerospace Structures and Materials Laboratory and the technician team for providing laboratory equipment and useful technical support. Also, the authors would like to gratefully acknowledge the support from TASS International by providing them with the license for MADYMO and supporting the model implementation. In addition, sincere appreciation to Mr. David Arterburn from the ASSURE research group and its partner's university for providing them with data and video footage of the UAS impact drop test which was used for model validation.

Disclosure statement

No potential conflict of interest was reported by the authors.

ORCID

Borrdephong Rattanagraikanakorn http://orcid.org/0000-0002-1489-8777
Riender Happee http://orcid.org/0000-0001-5878-3472

References

[1] European Aviation Safety Agency. Prototype Commission Regulation on Unmanned Aircraft Operations [Internet]; 2016 [Accessed on 2017 May 30]. Available from: https://www.easa.europa.eu/system/files/dfu/UAS Prototype Regulation final.pdf.

[2] European Aviation Safety Agency (EASA). Drone Collision Task Force [Internet]; 2016 [Accessed on 2017 Feb 17]. Available from: https://www.easa.europa.eu/system/files/dfu/TF Drone Collision_Report for Publication %28005%29.pdf.

[3] Civil Aviation Safety/Monash University. Human injury model for small unmanned aircraft impacts [Internet]. Canberra; 2013 [Accessed on 2017 June 15]. Available from: http://casa.gov.au/sites/g/files/net351/f/_assets/main/airwort/papers/human-injury-model-small-unmanned-aircraft-impacts.pdf.

[4] Magister T. The small unmanned aircraft blunt criterion based injury potential estimation. Saf Sci. [Internet] 2010;48:1313–1320. doi:10.1016/j.ssci.2010.04.012.

[5] Arterburn DR, Duling CT, Goli NR. Ground collision severity standards for UAS operating in the National Airspace System (NAS). 17th AIAA Aviation Technology, Integration, and Operations Conference [Internet]. 2017 [Accessed on 2018 Nov 18]. p. 1–16. Available from: https://arc.aiaa.org/doi/10.2514/6.2017-3778.

[6] Arterburn D, Ewing M, Prabhu R, et al. FAA UAS Center of Excellence Task A4: UAS ground collision severity evaluation [Internet]. Huntsville; 2017 [Accessed on 2018 Nov 18]. Available from: http://www.assureuas.org/projects/deliverables/a4/ASSURE_A4_Final_Report_UAS_Ground_Collision_Severity_Evaluation.pdf.

[7] Huculak R. NIAR UAS drop testing report [Internet]. Wichita; 2016 [Accessed on 2018 May 04]. Available from: http://www.assureuas.org/projects/deliverables/a11/NIAR Test Report – FAA-UAH UAS Drop Testing.pdf.

[8] Koh CH, Deng C, Li L, et al. Experimental and simulation weight threshold study for safe drone operations. AIAA Inf Syst Infotech Aerospace 2018;2018:1–11.

[9] Koh CH, Low KH, Li L, et al. Weight threshold estimation of falling UAVs (unmanned aerial vehicles) based on impact energy. Transp Res Part C Emerg Technol. [Internet] 2018;93:228–255. doi:10.1016/j.trc.2018.04.021.

[10] Campolettano ET, Bland ML, Gellner RA, et al. Ranges of injury risk associated with impact from unmanned aircraft systems. Ann Biomed Eng. [Internet] 2017;45(12):2733–2741. Available from: http://link.springer.com/10.1007/s10439-017-1921-6.

[11] Vadlamudi S, Blundell M, Zhang Y. A multi-body systems approach to simulate helicopter occupant protection systems. International Journal of Crashworthiness. 2011;16:207–218.Available from: http://www.tandfonline.com/doi/ref/10.1080/13588265.2011.554203?scroll=top.

[12] Jenefeldt F, Thomson R. A methodology to assess frontal stiffness to improve crash compatibility. Int J Crashworthiness. 2004;9:475–482.

[13] Mukherjee S, Chawla A, Nayak A, et al. Rollover crashworthiness of a rural transport vehicle using MADYMO. Int J Crashworthiness. 2006;11:495–503.

[14] Ambrósio J, Dias J. A road vehicle multibody model for crash simulation based on the plastic hinges approach to structural deformations. Int J Crashworthiness. 2007;12:77–92.

[15] Laananen DH, Bolukbasi AO, Coltman JW. Computer Simulation of an Aircraft Seat and Occupant in a Crash Environment [Internet]. 1983 [Accessed on 2017 Feb 05]. Available from: http://www.dtic.mil/docs/citations/ADA127152%5Cnhttp://www.dtic.mil/dtic/tr/fulltext/u2/a127152.pdf%5Cnhttp://www.dtic.mil/get-tr-doc/pdf?AD=ADA127152.

[16] TASS International. MADYMO theory manual version 7.7. MADYMO utilities manual. TASS International. Helmond, The Netherlands. 2017.

[17] Alliance for System Safety of UAS through Research Excellence. ASSURE UAS Ground Collision Severity Evaluation Final Report [Internet]. [cited 2018 Nov 18]. Available from: http://www.assureuas.org/projects/deliverables/sUASGroundCollisionReport.php.

[18] Adams V, Askenazi A. Building better products with finite element analysis [Internet]. OnWord Press; 1999 [Accessed on 2017 April 28]. Available from: https://books.google.nl/books?id=Mnv6qRz73x0C.

[19] Happee R, Hoofman M, Van Den Kroonenberg AJ, et al. A mathematical human body model for frontal and rearward seated automotive impact loading. SAE Tech Paper 983150. 1998. doi:10.4271/983150

[20] Happee R, Ridella S. Mathematical human body models representing a mid size male and a small female for frontal, lateral and rearward impact loading. IRCOBI Conference Proceedings, Bron, France. 2000. p 1–18.

[21] TASS International. Human body models manual version 7.7. TASS International. Helmond, The Netherlands. 2017.

[22] TASS International. Model manual version 7.7. TASS International. Helmond, The Netherlands. 2017.

[23] Brake MR. An analytical elastic-perfectly plastic contact model. Int J Solids Struct. [Internet] 2012;49:3129–3141. doi:10.1016/j.ijsolstr.2012.06.013.

[24] MATBASE. Matbase: the independent online material selection resource [Internet]. [cited 2017 Sep 3]. Available

from: https://www.matbase.com/material-categories/natural-and-synthetic-polymers/thermoplastics/commodity-polymers/material-properties-of-acrylonitrile-butadiene-styrene-general-purpose-gp-abs.html#properties.
[25] Lozano-Mínguez E, Palomar M, Infante-García D, et al. Assessment of mechanical properties of human head tissues for trauma modelling. Int J Numer Method Biomed Eng. 2018;34:1–17.
[26] Hutchinson J, Kaiser MJ, Lankarani M. The head injury criterion (HIC) functional. J Appl Math Comput. 1998;96(1):1–16.
[27] Eppinger R, Sun E, Bandak F, et al. Development of improved injury criteria for the assessment of advanced automotive restraint systems – II By [Internet]. 1999 [Accessed on 2018 March 21]. Available from: https://www.nhtsa.gov/sites/nhtsa.dot.gov/files/rev_criteria.pdf.
[28] Klinich K, Saul R, Auguste G, et al. Techniques for developing child dummy protection reference values [Internet]. 1996 [Accessed on 2018 March 07]. Available from: http://www.rosap.ntl.bts.gov/view/dot/14741/dot_14741_DS1.pdf.
[29] Parr MJC, Miller ME, Bridges NR, et al. Evaluation of the Nij neck injury criteria with human response data for use in future research on helmet mounted display mass properties. Proc Hum Factors Ergon Soc. 2012;56:2070–2074.
[30] Mroz K, Bostrom O, Bengt P, et al. Comparison of Hybrid III and human body models in evaluating thoracic response for various seat belt and airbag loading conditions. IRCOBI Conference Sept 15–16, 2010. p. 265–280.
[31] Sances A, Kumaresan S. Comparison of biomechanical head-neck responses of hybrid III dummy and whole body cadaver during inverted drops. Biomed Sci Instrum. [Internet] 2001 [cited 2018 Oct 24];37:423–427. Available from: http://www.ncbi.nlm.nih.gov/pubmed/11347428.
[32] Sances A, Carlin F, Kumaresan S. Biomechanical analysis of head-neck force in hybrid III dummy during inverted vertical drops. Biomed Sci Instrum. [Internet] 2002 [cited 2018 Oct 24];38:459–464. Available from: http://www.ncbi.nlm.nih.gov/pubmed/12085650.
[33] Mueller B, MacAlister A, Nolan J, et al. Comparison of HIC and BrIC head injury risk in IIHS frontal crash tests to real-world head injuries. Enhanc Saf Veh. 2015;1–18.
[34] Wei L, Griffin J. The prediciton of seat transmissibility from measures of seat impedance. J Sound Vib. [Internet] 1998 [cited 2019 Apr 30];214:121–137. Available from: https://www.sciencedirect.com/science/article/pii/S0022460X98915401.

Appendix A. Effect of component stiffness on head force

This preliminary study is to determine the difference in impact force on the human head due to UAS collision at different point of contact on the DJI Phantom III UAS. Head acceleration resulted from UAS collision from three different contact points (Frontal contact, camera gimbal and landing gear) are modelled and compared using a simplified lumped parameter mass (LPM) model as shown in Figure A3. Each point of contact has different stiffness which affects the impact force between a UAS and the human head.

Figure A2 shows the force–deformation curves of a different point of contact. Frontal contact force–deformation curve was approximated using modified Hertz contact [23]. Camera gimbal and landing gear force–deformation curves were measured experimentally using static compressive test as shown in Figure A1. Frontal contact (main fuselage body) is the stiffest point of contact with a stiffness value of approximately 83,000 N/m. Camera gimbal has a stiffness of approximately 35,000 N/m. The landing gear is the softest component with the stiffness of 15,625 N/m.

To assess head-acceleration, the simplified LPM UAS-human head model was developed. The human head/neck LPM model is from the work by Wei and Griffin [34]. UAS is lumped into one lumped mass with a spring representing the components (frontal contact, camera gimbal and landing gear). Stick assumption was applied, meaning that the UAS is attached to the head after the collision. The model was run for 0.016 s at UAS impact velocity of 18 m/s (maximum UAS speed). The modelling results are shown in Figure A4. The figure shows that frontal contact results in the highest head force with a peak force of more than 17,700 N. Gimbal contact results in the peak force of approximately 9000 N. Landing gear, which is the softest component, results in the head force of less than 4300 N.

Figure A1. Static compressive test to determine the force–deformation curve of each component.

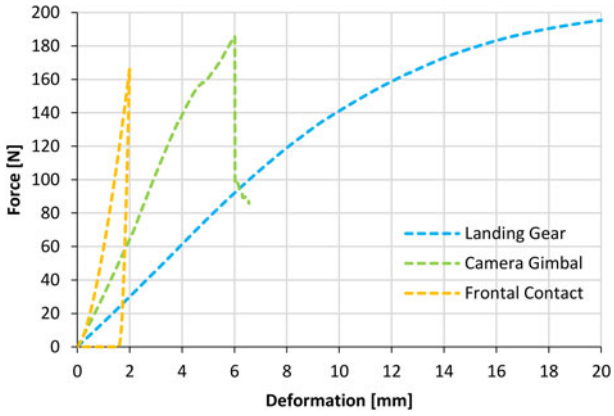

Figure A2. Force–deformation curve of three different points of contact.

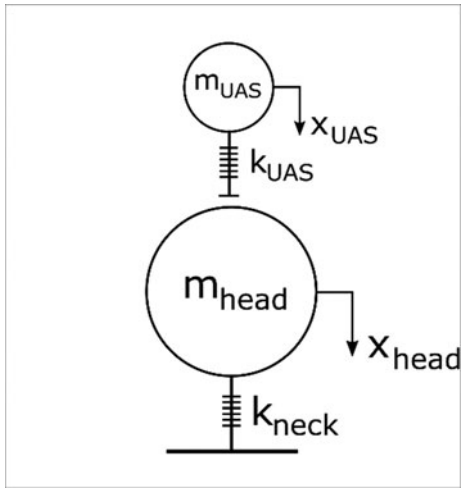

Figure A3. Simplified UAS–head lumped parameters model. Head/neck mass and stiffness is from the work by Wei and Griffin [34].

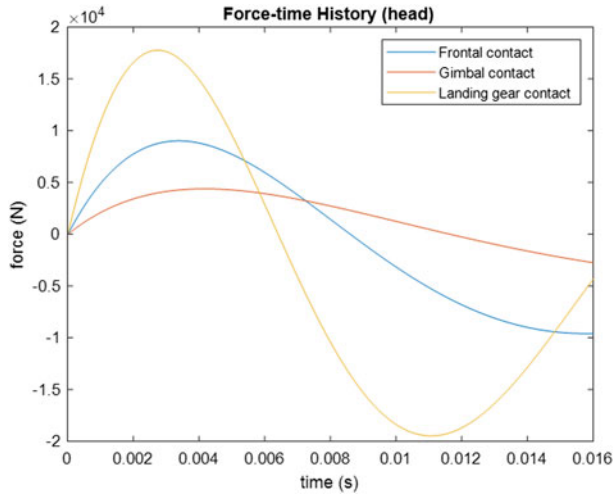

Figure A4. Force–time history of the human head at head CG due to UAS impacts with different point of contacts at impact velocity of 18 m/s.